JOURNAL OF GEOPHYSICAL RESEARCH, VOL. 115, D13305, doi:10.1029/2009JD013503, 2010

Click Here for Full Article

# Direct Sun measurements of $NO_2$ column abundances from Table Mountain, California: Intercomparison of low- and high-resolution spectrometers

Shuhui Wang,[1] Thomas J. Pongetti,[1] Stanley P. Sander,[1] Elena Spinei,[2] George H. Mount,[2] Alexander Cede,[3] and Jay Herman[4]

Received 4 November 2009; revised 3 March 2010; accepted 10 March 2010; published 15 July 2010.

[1] The $NO_2$ total column abundance, $C_{NO_2}$, was measured with a direct Sun viewing technique using three different instruments at NASA Jet Propulsion Laboratory's (JPL) Table Mountain Facility in California during an instrument intercomparison campaign in July 2007. The instruments are a high-resolution (~0.001 nm) Fourier transform ultraviolet spectrometer (FTUVS) from JPL and two moderate-resolution grating spectrometers, multifunction differential optical absorption spectroscopy (MF-DOAS) (~0.8 nm) from Washington State University and Pandora (~0.4 nm) from NASA Goddard Space Flight Center. FTUVS uses high spectral resolution to determine the absolute $NO_2$ column abundance independently from the exoatmospheric solar irradiance using rovibrational $NO_2$ absorption lines. The $NO_2$ total column is retrieved after removing the solar background using Doppler-shifted spectra from the east and west limbs of the Sun. The FTUVS measurements were used to validate the independently calibrated measurements of multifunction differential optical absorption spectroscopy (MF-DOAS) and Pandora. The latter two instruments start with measured high-Sun spectra as solar references to retrieve relative $NO_2$ columns and then apply modified Langley or "bootstrap" methods to determine the amounts of $NO_2$ in the references to obtain the absolute $NO_2$ columns. The calibration offset derived from the FTUVS measurements is consistent with the values derived from Langley and bootstrap calibration plots of the $NO_2$ slant column measured by the grating spectrometers. The calibrated total vertical column abundances of $NO_2$, $C_{NO_2}$, from all three instruments are compared showing that MF-DOAS and Pandora data agree well with each other, and both data sets agree with FTUVS data to within (1.5 ± 4.1)% and (6.0 ± 6.0)%, respectively.

**Citation:** Wang, S., T. J. Pongetti, S. P. Sander, E. Spinei, G. H. Mount, A. Cede, and J. Herman (2010), Direct Sun measurements of $NO_2$ column abundances from Table Mountain, California: Intercomparison of low- and high-resolution spectrometers, *J. Geophys. Res.*, *115*, D13305, doi:10.1029/2009JD013503.

## 1. Introduction

[2] Nitrogen dioxide ($NO_2$) is closely related to atmospheric $O_3$ production and loss. In the upper troposphere and stratosphere, $NO_2$ plays a role in the catalytic destruction of $O_3$ [*Logan et al.*, 1981; *Brasseur et al.*, 1998; *Crutzen*, 1970]. In the troposphere, $NO_2$ from both anthropogenic emissions and natural sources are precursors of tropospheric $O_3$, largely through reactions with hydrocarbons [e.g., *Murphy et al.*, 1993]. The tropospheric $NO_2$ level and distribution directly affect air quality [e.g., *Seinfeld and Pandis*, 1998]. Measurements of $NO_2$ abundance seasonally and diurnally are thus important to the understanding of tropospheric and stratospheric chemistry.

[3] Total column abundance measurements of $NO_2$ ($C_{NO_2}$) have been made from space by a number of satellite-based instruments, e.g., the Global Ozone Monitoring Experiment (GOME) since 1995, the Scanning Imaging Absorption Spectrometer from Atmospheric Cartography (SCIAMACHY) since 2002, and the Ozone Monitoring Instrument (OMI) on board Aura since 2004 [*Boersma et al.*, 2007; *Bucsela et al.*, 2006; *van der A et al.*, 2008; *Wenig et al.*, 2004]. One of the key steps in the satellite data retrieval is to convert the measured trace gas slant column densities into vertical column densities through the air mass factor (AMF). The AMF is calculated using radiative transfer models that account for

[1]Jet Propulsion Laboratory, California Institute of Technology, Pasadena, California, USA.
[2]Laboratory for Atmospheric Research, Department of Civil and Environmental Engineering, Washington State University, Pullman, Washington, USA.
[3]Earth System Science Interdisciplinary Center, University of Maryland, College Park, Maryland, USA.
[4]NASA Goddard Space Flight Center, Greenbelt, Maryland, USA.

Copyright 2010 by the American Geophysical Union.
0148-0227/10/2009JD013503

optical geometry, surface reflectivity, clouds and aerosol properties, and the vertical distribution of the absorbing trace gas.

[4] The validation of satellite measurements of $C_{NO_2}$ is often done through comparison with ground-based measurements at various locations [e.g., *Ionov et al.*, 2008; *Wenig et al.*, 2008; *McPeters et al.*, 2008; *Kramer et al.*, 2008; *Celarier et al.*, 2008; *Herman et al.*, 2009]. There are a number of techniques to measure $C_{NO_2}$ using ground-based instruments. Multiaxis differential optical absorption spectroscopy (MAX-DOAS) measures the scattered skylight spectrum over a range of viewing angles from nearly horizontal to zenith, providing both total and tropospheric $C_{NO_2}$ [*Platt and Stutz*, 2008; *Hönninger et al.*, 2004; *Wittrock et al.*, 2004]. The major challenge in the MAX-DOAS method is determination of the AMF, which depends on observational parameters that are often difficult to accurately determine, e.g., aerosol loading and the vertical profile shape.

[5] Direct Sun DOAS (DS-DOAS) is another technique to measure $C_{NO_2}$ from the ground [*Herman et al.*, 2009; *Cede et al.*, 2006; *Brewer et al.*, 1973]. Since the unscattered solar irradiance is measured at a known solar zenith angle (SZA), the conversion factor from slant column to vertical column for DS-DOAS is geometrically determined as approximately sec (SZA) and does not require sophisticated radiative transfer models. While the absolute $C_{NO_2}$ should be determined from the exoatmospheric solar irradiance spectrum ($I_0$) at the top of the atmosphere convolved with the spectrometer's point-spread function and then ratioed to the measured spectrum of a particular observation (equivalent to a spectrum free of $NO_2$ absorption), $I_0$ is not directly accessible; however, absolute $C_{NO_2}$ can be obtained using field calibration techniques, e.g., the commonly used Langley extrapolation method [*Roscoe et al.*, 1999] and its modified version, minimum-amount Langley extrapolation (MLE) [*Herman et al.*, 2009].

[6] Recently a technique employing high-resolution direct Sun spectroscopy with solar Doppler differencing has been developed to measure absolute $C_{NO_2}$ without the need for $I_0$ (T. J. Pongetti et al., Retrieval of $NO_2$ absolute columns in the stratosphere and troposphere from ground-based UV-visible measurements with the Fourier transform ultraviolet spectrometer (FTUVS) at Table Mountain, manuscript in preparation, 2010). This method uses the Jet Propulsion Laboratory (JPL) high-resolution Fourier transform ultraviolet spectrometer (FTUVS) instrument [*Cageao et al.*, 2001] to measure the Doppler-shifted solar lines from the east and west limbs of the rotating Sun. The advantage of high spectral resolution and the dual solar limb measurements is that the unknown $I_0$ is canceled out (see details in section 2.1). Thus, the field calibration techniques required for DS-DOAS to account for the amount of $NO_2$ in the high-Sun reference are not needed for the FTUVS. It is therefore an absolute $NO_2$ measurement technique which does not require the determination of the $NO_2$-free exoatmospheric solar irradiance.

[7] During an intercomparison field campaign in July 2007, three direct Sun viewing instruments, a high-resolution FTUVS (~0.001 nm) from JPL and two low-resolution (~0.8 nm and ~0.4 nm) spectrometers (multifunction differential optical absorption spectroscopy (MF-DOAS) from Washington State University and Pandora from NASA Goddard Space Flight Center (GSFC)), were operated side-by-side to measure $C_{NO_2}$ from the Table Mountain Facility (TMF) (34.4°N, 117.7°W) in California. The absolute measurement results from the FTUVS are used to validate the calibration of the other two instruments, which utilize high-Sun references followed by application of the modified Langley or "bootstrap" methods to determine the $NO_2$ absolute column amounts [*Herman et al.*, 2009]. The independent results from all methods are compared and shown to agree. The calibrated absolute columns $C_{NO_2}$ from all instruments during this campaign are presented. The intercomparison is discussed in detail.

## 2. Direct Sun $NO_2$ Measurement Techniques

### 2.1. FTUVS Description

[8] The JPL FTUVS has been measuring the vertical column abundance of trace species over TMF under clear to lightly cloudy sky conditions since 1997 [*Cageao et al.*, 2001; *Li et al.*, 2005; *Mills et al.*, 2002; *Wang et al.*, 2008; *Cheung et al.*, 2008; Pongetti et al., manuscript in preparation, 2010]. $NO_2$ measurements started in 2005. It has a broad spectral coverage, ranging from 4000 $cm^{-1}$ to 40,000 $cm^{-1}$ and a resolving power of over 500,000. The spectral resolution is 0.06 $cm^{-1}$ (on the order of 0.001 nm at 400 nm). The instrument system contains three subsystems: a heliostat for tracking the Sun, a beam defining telescope, and an interferometer. The details of the instrument design and parameters are described by *Cageao et al.* [2001]. For $NO_2$ measurements, a narrow-band-pass filter with a band-pass range of 488–498 nm (20,100–20,500 $cm^{-1}$) is placed at the entrance to the interferometer to improve the signal-to-noise ratio, which is typically a few thousand for a single scan. The details of the data acquisition and data reduction methods are given by Pongetti et al. (manuscript in preparation, 2010).

[9] The most important advantage of high-resolution solar absorption spectroscopy for $C_{NO_2}$ is that the unknown exoatmospheric solar irradiance ($I_0$) can be removed using the Doppler differencing method [*Cageao et al.*, 2001], thus eliminating the need for external calibration. During each measurement cycle, high-resolution spectra from the east and west limbs of the Sun are taken alternately (17 min integration time for each limb). While solar spectral lines are Doppler shifted between the east and west limb spectra (about 0.28 $cm^{-1}$), $NO_2$ lines from the Earth's atmosphere remain unshifted. By matching and ratioing a pair of spectra (east limb spectrum divided by the west limb spectrum that is spectrally shifted to match the east limb), in principle, solar features are canceled out, leaving only terrestrial $NO_2$ absorption features. The examples in Figures 1a, 1b, 1e, and 1f illustrate the matching and ratioing steps of the measured spectra. This Doppler shift method has been used to successfully retrieve other trace species such as OH [*Cageao et al.*, 2001; *Iwagami et al.*, 1995]. Since each limb spectrum is paired with the opposite limb spectra taken before and after it to generate two data points, the recorded time interval for FTUVS measurements is about 17 min although each independent measurement cycle covers a period of at least 34 min.

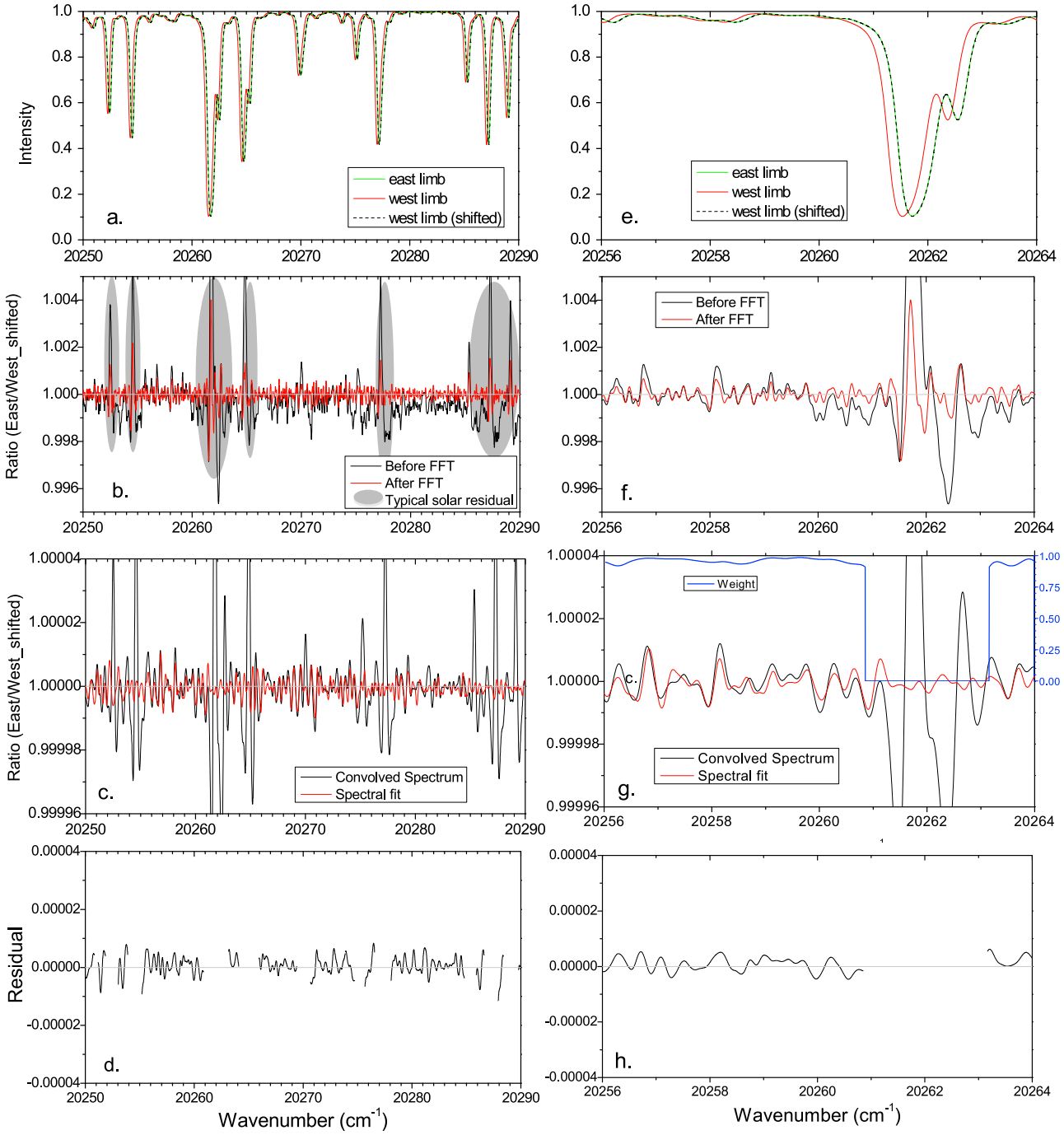


**Figure 1.** Illustration of the $NO_2$ spectral retrieval steps. (left) Columns show examples in a 40 wave number–wide spectral window and (right) details in a smaller window. (a and e) The east and west limb solar spectra and the shifted west limb solar spectrum. The shift matches the solar lines from the opposite limbs that are Doppler shifted. The $NO_2$ lines that are not subject to Doppler shift are thus shifted after this step. (b and f) The ratio of the east limb solar spectrum and the shifted west limb solar spectrum before and after the high-pass FFT filter, which shows $NO_2$ features on top of strongly attenuated solar features. The ratio after high-pass FFT filter shows a flat background while the one before filter has a broad-bond solar baseline feature. (c and g) The weighted fit after the convolution at 2 atm and (d and h) the residuals are also shown.

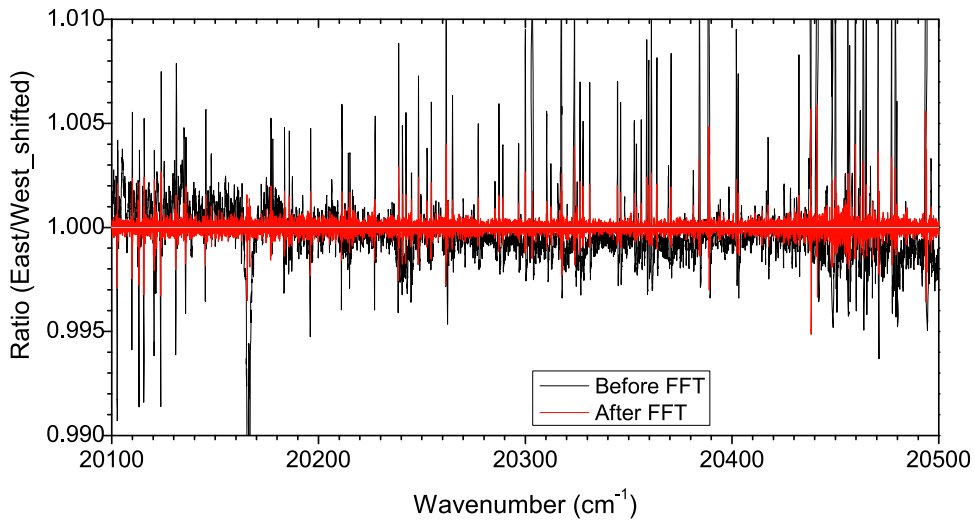


**Figure 2.** Overview of the effect of the high-pass FFT filter in removing broadband background features.

[10] In practice, the solar features are strongly attenuated in the ratio but not completely removed because of the asymmetry of the Sun and the imperfection of the shift-and-ratio procedure. In the spectral window for $NO_2$ retrieval, the remaining solar features have two major components, a broadband solar baseline and the residual of each solar line. A fast Fourier transform (FFT) high-pass filter is applied to the ratioed spectra to remove the low-frequency solar baseline, leaving only high-frequency $NO_2$ lines and residual solar lines. Figures 1b and 1f show an example spectrum ratio before and after the FFT filter. To show the overall effect, the overview of the spectrum ratios before and after the FFT filter in the entire 400 wave number spectral window is plotted in Figure 2. The resulting spectrum ratio contains numerous high-frequency $NO_2$ rovibrational lines as well as the residual of each solar line (indicated by the sharp spikes). To avoid the interference from the solar line residual during the $NO_2$ spectral fit, a weighted fit is applied so that the spectral regions with strong solar residuals are masked out from the fit window. The weight is calculated on the basis of the strength and the shape of the solar lines (Pongetti et al., manuscript in preparation, 2010). It is unity where there is no influence from solar features and smaller elsewhere and zero where strong solar residual persists in the ratio (Figure 3). As a result of this weighted fit, numerous microwindows, each covering a number of $NO_2$ lines but including no effective solar lines, are selected from the original spectral window and are treated simultaneously during the least squares spectral fit.

[11] The $NO_2$ reference spectra used in the spectral fit are taken from the laboratory study of *Nizkorodov et al.* [2004]. In this study, $NO_2$ cross sections were measured using the McMath Fourier transform spectrometer at the National Solar Observatory at high spectral resolution (0.06 $cm^{-1}$) over a range of pressures and temperatures relevant to atmospheric conditions. The shape and the depth of $NO_2$

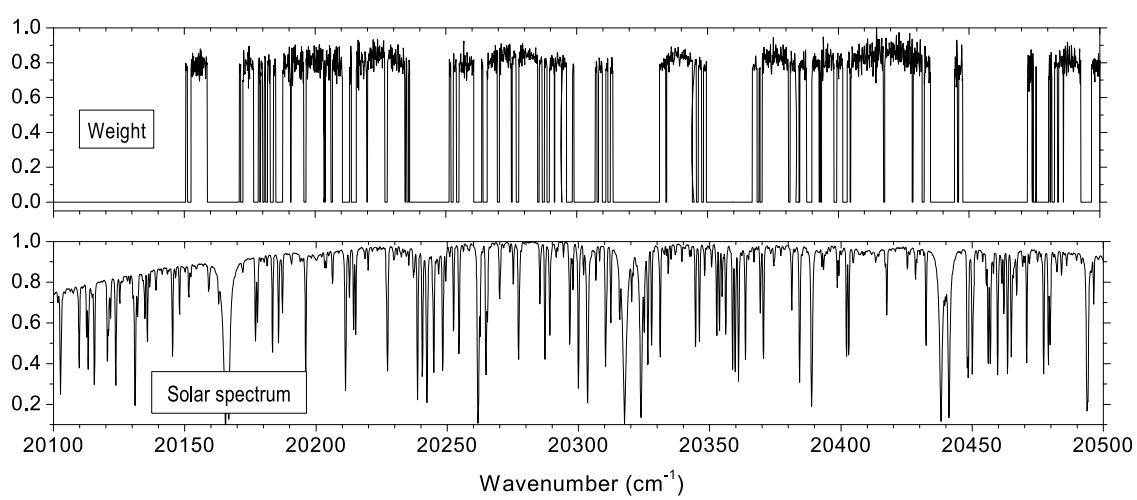


**Figure 3.** The weight applied during the $NO_2$ spectral fit in comparison to the original solar spectrum. Where the solar lines are strong and a strong solar residual may occur in the spectrum ratio, the weight goes to zero so that these regions are masked out during the $NO_2$ spectral fit.

**Table 1.** Side-by-Side Comparison of the Three Direct Sun Instruments

| | FTUVS | MF-DOAS | Pandora |
|---|---|---|---|
| Instrument spectral range | 488–498 nm | 282–498 nm | 265–500 nm |
| Spectral window for $NO_2$ fit | 488–498 nm | 405–430 nm | 370–500 nm |
| Spectral resolution | ~0.001 nm | ~0.8 nm | ~0.4 nm |
| Total integration time | 17 min | 20 ms–60 s | 20 s |
| Number of scans per cycle | 40 | 1 | 50–2500 |
| Spectral sampling of the grating spectrometers | | 7.8 pixels per FWHM | 3 pixels per FWHM |

absorption lines are strongly pressure broadened and are also sensitive to temperature. Using interpolation formulae determined by *Nizkorodov et al.* [2004], the $NO_2$ cross sections at any atmospheric pressure and temperature can be derived. In the current retrieval algorithm, the atmosphere is divided into 21 layers. The $NO_2$ reference spectrum in each layer is derived according to the corresponding pressure and temperature. With assumed a priori profiles of $NO_2$ in the stratosphere and the troposphere (Pongetti et al., manuscript in preparation, 2010), the weighted average $NO_2$ references in the stratosphere and the troposphere are calculated. These references are processed using the same procedures that are applied to the measured spectra to remove the solar features (e.g., the ratio of shifted spectra and the application of a FFT filter). The reference for the total column in the atmosphere is derived on the basis of an estimated $NO_2$ partition between stratosphere and troposphere (3:1 for this field campaign, according to the multiyear measurements at TMF during this time of year and with similar meteorological conditions).

[12] Because FTUVS records the $NO_2$ spectrum with a spectral resolution that resolves the pressure-broadened $NO_2$ lines, the resulting $NO_2$ line shapes carry information about the vertical concentration profile. Since we are comparing the measurements of the $NO_2$ total column between instruments, it is desirable to remove the sensitivity of the FTUVS retrievals to the measured and a priori vertical profiles. To accomplish this, both measured and reference spectra are convolved to high pressure (2 atm, empirically selected as the optimal pressure level for this convolution) so that the sensitivity to vertical profile information is minimized (Pongetti et al., manuscript in preparation, 2010). The equivalent effective spectral resolution after this convolution is about 0.24 $cm^{-1}$. Note that while a higher pressure helps to further reduce vertical profile information, it smears $NO_2$ spectral features. With this approach, the systematic error in absolute $NO_2$ column arising from the assumed a priori $NO_2$ partitioning between the stratosphere and troposphere varies from a couple percent to up to ten percent when tropospheric $NO_2$ is as large as or even higher than stratospheric $NO_2$, a condition uncommon at this time of year at TMF (Pongetti et al., manuscript in preparation, 2010). An example of the weighted spectral fit after convolution and the corresponding residuals is shown in Figures 1c, 1d, 1g, and 1h. The selected window includes one of the strongest solar lines, which is excluded from the fit by the zero weight (blue line).

[13] The spectral analysis described above generates the absolute slant column abundances of $NO_2$, $SC_{NO_2}$, which are easily converted into vertical column abundances, $C_{NO_2}$, through the geometrically determined SZAs. These absolute ($I_0$-independent) measurements of $C_{NO_2}$ during the instrument intercomparison campaign thus provide an independent approach to validate the field calibration of the other instruments that were operated simultaneously.

## 2.2. MF-DOAS and Pandora Description

[14] The two grating spectrometers, multifunction differential optical absorption spectroscopy (MF-DOAS) and Pandora, are both array detector (CCD and complementary metal oxide semiconductors (CMOS)) instruments. They have been deployed during a number of recent campaigns at various sites, providing both short-term and long-term (multiyear) $NO_2$ data for OMI validation [e.g., *Herman et al.*, 2009]. The MF-DOAS system is based on an extensively reworked 30 cm focal length Acton SP-2300i single-pass Czerny-Turner spectrograph with a back illuminated UV-coated rectangular CCD detector (512 pixels × 2048 pixels). The spectral range covered is 282–498 nm with a spectral resolution of ~0.8 nm and a spectral sampling of 7.8 CCD pixels per full width at half maximum (FWHM) of a spectral feature. The spectral fitting for $NO_2$ measurements uses the window between 405–460 nm. Typical integration times are on order of 1 s with excellent signal-to-noise ratio and precision. The Pandora spectrometer uses an Avantes symmetrical Czerny-Turner optical design with a focal length of 7.5 cm. The 1200 lines per millimeter diffraction grating provides a spectral range from 265 to 500 nm with a spectral resolution of ~0.4 nm and a spectral sampling of 3 CMOS pixels per FWHM. A spectral fitting window of 370–500 nm was selected for $NO_2$. The CMOS detector is a low-noise 1024 pixel Hamamatsu linear array. The larger CCD and longer focal length of the MF-DOAS are the two main features that give MF-DOAS improved precision, for a given exposure time, compared to the Pandora instrument for direct Sun observations. More details about the instrument design and operation are given by *Herman et al.* [2009]. A side-by-side comparison of these instruments and FTUVS is shown in Table 1.

[15] The $NO_2$ retrieval method for this type of direct Sun instrument has been described in detail by *Herman et al.* [2009]. The retrieval of MF-DOAS and Pandora data uses a similar method, with different spectral ranges. The $NO_2$ absolute absorption cross sections used in the spectral fit are

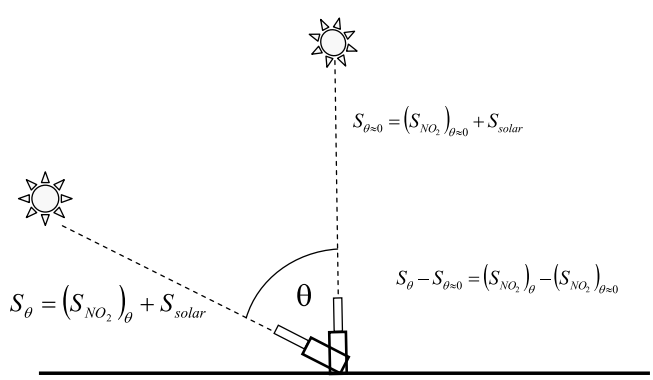


**Figure 4.** Schematics of the $NO_2$ retrieval method for low-resolution direct Sun spectrometers.

derived from moderately high spectral resolution (0.003 nm) laboratory measurements [*Harder et al.*, 1997] assuming a weighted column average atmospheric temperature of 238 K at TMF. The uncertainty introduced by this assumption is expected to be small and will be discussed in section 5.4.

[16] Since the exoatmospheric solar irradiance ($I_0$) cannot be directly determined by ground-based instruments, both MF-DOAS and Pandora use a measured clean day high-Sun spectrum, which contains the smallest $SC_{NO_2}$, as reference spectra for their initial $NO_2$ retrieval for all the campaign data. As illustrated in Figure 4, the spectral signal measured at a SZA of $\theta$, $S_\theta$, is a combination of $NO_2$ slant column absorption signal $(S_{NO_2})_\theta$ and the exoatmospheric solar irradiance $S_{solar}$ (or $I_0$). During the initial retrieval, the selected high-Sun spectrum ($S_{\theta\approx 0}$) is used to cancel out $S_{solar}$ (or $I_0$), generating a relative $SC_{NO_2}$, which is the difference between the two absolute slant columns $(S_{NO_2})_\theta$ and $(S_{NO_2})_{\theta\approx 0}$. During this TMF field campaign, the initial reference spectrum for each instrument was selected from measurements obtained at local noon on 7 July 2007, a day with very small tropospheric $NO_2$ column abundances above TMF.

[17] To calculate the absolute slant columns from these retrieved relative slant columns, the amount of $NO_2$ in the high-Sun reference has to be determined by calibration. This necessary calibration of the reference slant columns can be derived using MLE or bootstrap estimate (BE) methods as described by *Herman et al.* [2009]. Comparisons of these relative slant columns with simultaneous FTUVS measurements provide an independent calibration that can be used to validate the above-mentioned field calibration techniques. Section 4 will discuss the calibration using FTUVS data and its comparison to two other calibration methods used on the MF-DOAS and Pandora data, MLE and BE [*Herman et al.*, 2009].

## 3. Overview of Measurement Results

[18] Figure 5 shows an overview of $SC_{NO_2}$ (open circles) and $C_{NO_2}$ (solid squares) from FTUVS absolute measurements during the 11 day field campaign. Since the FTUVS observations require clear or lightly cloudy conditions, the periods with heavy clouds are marked (dark gray shading in Figure 5) and excluded from the discussions beyond this point. There were also periods when the FTUVS results were judged to be unreliable, mainly because of alignment problems associated with the recent replacement of the instrument's reference laser. The misalignment problems were found to correlate with the laboratory temperature, which was part of the data archive. Data associated with periods of misalignment were highlighted in Figure 5 (light gray shading) and also excluded from consideration. A more detailed description of the exclusion of questionable data is provided in the auxiliary material.[1]

[19] The relative $SC_{NO_2}$ measurements from MF-DOAS and Pandora show excellent agreement. The one-to-one correlation scatterplot of the two data sets during the entire campaign is shown in Figure 6. The Pandora $SC_{NO_2}$ data were averages of measurements over about 3 min. To facilitate the comparisons, the MF-DOAS data (averaged over 1 min to avoid overcrowding) were linearly interpolated to the corresponding Pandora measurement time. The linear fit shows an excellent correlation coefficient of 0.993. The slope of 1.05 (with a small intercept of $-2.65 \times 10^{14}$ cm$^{-2}$) suggests that the agreement between these two data sets is within 5%, with Pandora slant columns being slightly larger than those from MF-DOAS.

## 4. Calibration Methods

### 4.1. Calibration Against FTUVS Absolute Measurements

[20] During the TMF intercomparison campaign, FTUVS, MF-DOAS, and Pandora were operated simultaneously to measure $NO_2$ column abundances. The FTUVS measured the absolute slant columns at any given time $t$, $SC(t)$, while the other spectrometers measured the relative slant columns, $SC_{rel}(t)$ before the field calibration. The difference between $SC(t)$ and $SC_{rel}(t)$ should be the slant column in the high-Sun reference, $SC_{ref}$, which is a constant:

$$SC_{rel}(t) = SC(t) - SC_{ref}. \quad (1)$$

[21] The scatterplot in Figure 7 shows the linear correlation of the relative slant columns from MF-DOAS and Pandora versus the absolute slant columns from FTUVS during this campaign. As mentioned earlier, since the time interval of FTUVS data is about 17 min, the raw data from the other two instruments were averaged for 17 min periods around the center of each FTUVS measurement cycle. The solid and the dash-dotted line are the linear fits of MF-DOAS and Pandora data versus FTUVS data, respectively. Both fits show an excellent correlation, with the coefficient $R$ being 0.96 and 0.94 for MF-DOAS and Pandora, respectively. The slopes are $1.04 \pm 0.02$ and $1.09 \pm 0.03$ for MF-DOAS and Pandora data sets, which again suggests that Pandora data are slightly higher than MF-DOAS as shown in Figure 6. As indicated in equation (1), the negative intercepts may be interpreted as the $SC_{NO_2}$ in the high-Sun references. For MF-DOAS and Pandora data sets, the intercepts in Figure 7 suggest the $SC_{NO_2}$ in the references to be $2.9 \pm 0.2 \times 10^{15}$cm$^{-2}$ (about $0.11 \pm 0.01$ Dobson unit (DU); 1 DU = $2.69 \times 10^{16}$ cm$^{-2}$) for both data sets.

[22] As mentioned earlier (section 2.1), when the tropospheric $NO_2$ contribution is significantly larger than 25% of the total column (the assumed partition between stratosphere and troposphere in FTUVS data retrieval), the total $NO_2$ column $C_{NO_2}$ would be slightly underestimated (from a couple percent to up to ten percent). On typical clean days, e.g., 6 July and 7 July 2007, the end-of-day $C_{NO_2}$ at TMF approaches 0.2 DU. Assuming that when observed $C_{NO_2}$ is over 0.2 DU the tropospheric $NO_2$ contribution is larger than our assumption, there are a total of less than 20 FTUVS data points that could have an underestimation. Sensitivity studies to estimate the associated impact on calibration results shown in Figure 7 were performed with these data points adjusted with a small increase of a couple of percent to ten percent followed by similar linear correlations. The intercepts resulting from such "adjusted" linear correlation studies have

[1]Auxiliary materials are available in the HTML. doi:10.1029/2009JD013503.

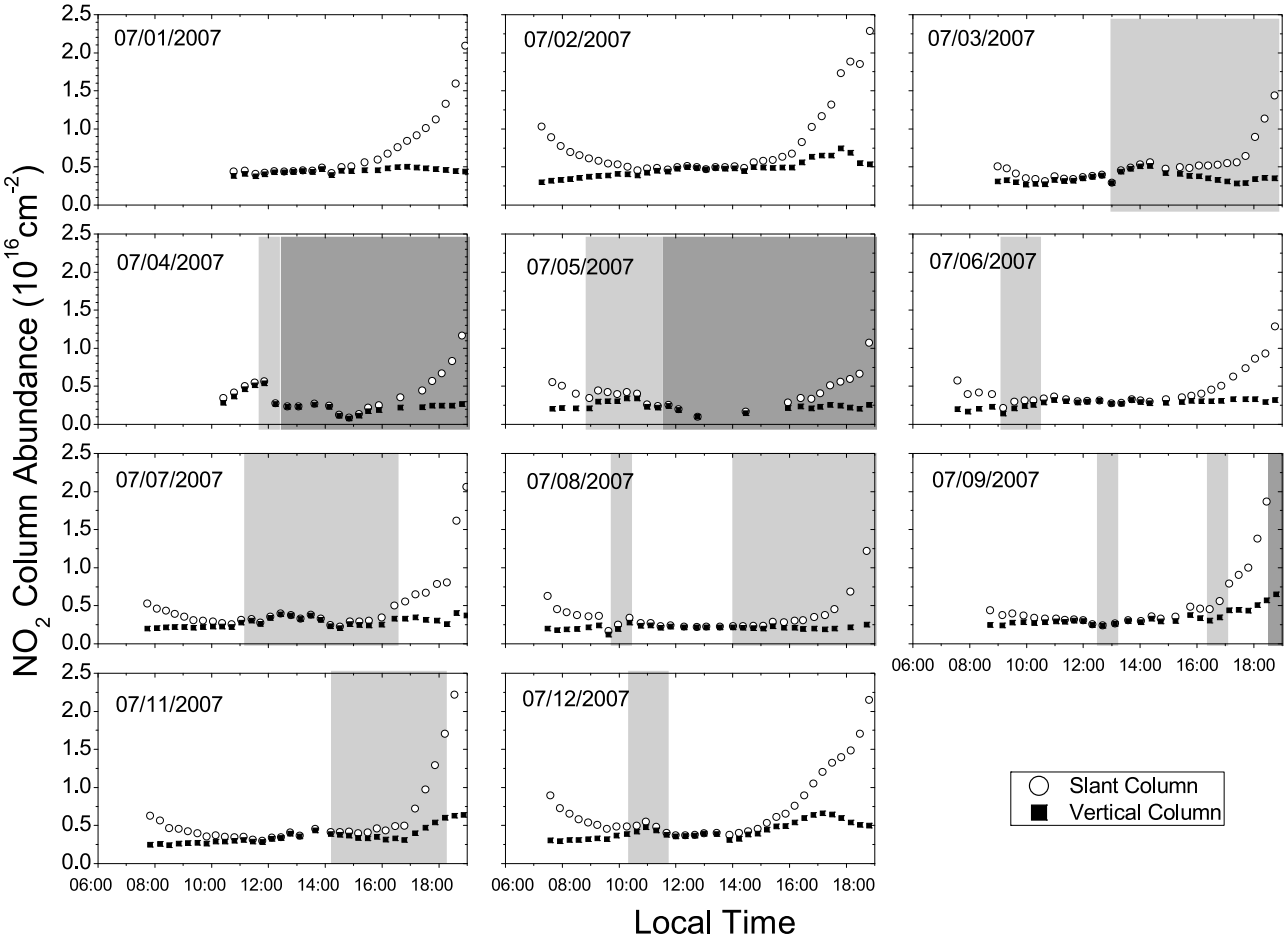


**Figure 5.** The overview of the FTUVS $NO_2$ absolute slant column and vertical column data during this field campaign. The questionable data points obtained during periods of instrument misalignment or heavy clouds were highlighted in light gray and dark gray, respectively. These data are excluded from the final results and discussions in this work.

values somewhat smaller than 0.11 DU with the lowest value being 0.10 DU. All these values are within the 0.11 ± 0.01 DU uncertainty range of the linear fits in Figure 7.

[23] While this linear correlation approach provides information about the amount of $NO_2$ in the high-Sun reference, the larger scatter range among fewer data points at high SZAs (corresponding to the points with high $NO_2$ slant columns) could potentially introduce bias to the fit. To avoid this possible bias, another statistical approach was also used to determine the reference. Equation (1) can be rearranged into the following equation (2). The reference is simply determined by the difference between the absolute slant columns from FTUVS, SC($t$), and the relative slant columns from the lower-resolution instruments, $SC_{rel}(t)$:

$$SC_{ref} = SC(t) - SC_{rel}(t). \quad (2)$$

The histograms of $SC(t) - SC_{rel}(t)$ for both data sets have shapes that are close to Gaussian distribution (Figure 8). The peak center of the Gaussian fits suggests that the amount of $NO_2$ in the high-Sun reference is about 0.10 DU for both data sets. These calibration results are the lower ends of the calibration ranges determined by the linear correlation of the slant columns (0.11 ± 0.01 DU). In the following discussion, the mean of values from these two methods is used for the calibration (i.e., 0.105 DU). The calibration uncertainty is estimated to be ~0.01 DU (0.01 DU divided by AMF for each vertical column data point). Further sensitivity studies show that a difference of 0.01 DU in calibration could contribute about 1% to the differences in $NO_2$ vertical columns among these measurements, which is not a significant source of differences.

### 4.2. Other Calibration Methods (Langley and Bootstrap)

[24] *Herman et al.* [2009] also described two other methods to calibrate these direct Sun instruments, MLE and BE. Both methods involve assumptions that may not be valid for the conditions of the intercomparison.

[25] The MLE method assumes that the minimum vertical column of $NO_2$ is independent of the AMF over some periods (e.g., a short period during a subset of the measurement days). Assuming that during periods with the lowest $C_{NO_2}$ the tropospheric $NO_2$ is negligible and the stratospheric $NO_2$ is a constant, $VC_0$, equation (1) can be rewritten as:

$$SC_{rel}(t) = SC(t) - SC_{ref} = VC_0[AMF(t)] - SC_{ref}. \quad (3)$$

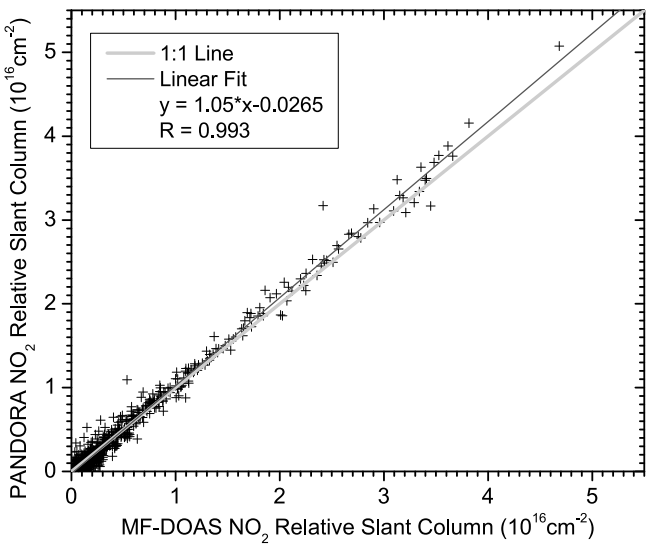


**Figure 6.** Linear correlation of $NO_2$ relative slant columns from MF-DOAS and Pandora during the campaign.

While the MLE assumption, i.e., the AMF-independent minimum vertical column, may or may not occur during a short campaign period at a polluted site, it is very likely to occur for longer-term (many months) measurements at a fixed location or for short campaigns at a clean site. TMF is generally a clean site with low tropospheric $NO_2$. This elevated observatory (2.25 km) is mostly free from the polluted air transported from the Los Angeles basin. The air column above TMF often has low tropospheric $NO_2$ as well as stable stratospheric $NO_2$ levels, which makes it an excellent location to calibrate direct Sun instruments with the Langley method. During this field campaign, 7 July appeared to be the day with the lowest amount of $NO_2$ and, thus, with conditions closest to the assumptions of the MLE method (and the BE method described below). The scatterplot of the retrieved relative $NO_2$ slant columns $SC_{rel}(t)$ versus AMF($t$) during this day should be close to a straight line with a slope of $VC_0$ and an intercept of $-SC_{ref}$. Using this method, $SC_{ref}$ for both MF-DOAS and Pandora were estimated to be 0.12 DU [*Herman et al.*, 2009], very close to the calibration with absolute FTUVS measurements (Table 2). The agreement between the MLE calibration using an 11 day campaign data set and the FTUVS calibration confirms that the tropospheric component of $NO_2$ during the selected measurement period at TMF was small.

[26] The BE method is also based on an assumption about $VC_0$. While the MLE method assumes a constant $VC_0$, the BE method assumes $VC_0$ to be 0.1 DU, the nominal mid-latitude stratospheric $NO_2$ column [*Herman et al.*, 2009]. Equation (2) is thus rewritten as

$$SC_{rel}(t) - VC_0[AMF(t)] = -SC_{ref}. \quad (4)$$

The left side of equation (4) is calculated using the data throughout the campaign and plotted as a histogram. The dominant distribution modes covering the majority of the data set should give a range of the value of $-SC_{ref}$. *Herman et al.* [2009] applied both MLE and BE methods to the TMF campaign data sets. The two methods were found to show similar calibration results, with the latter suggesting slightly larger $SC_{ref}$. The calibration results of $SC_{ref}$ with all methods are summarized in Table 2.

[27] Both MLE and BE methods agree with the calibration results using FTUVS measurements. The value of $SC_{ref}$ from MLE (0.12 DU) is very close to the value from the FTUVS calibration (0.105 DU), while the $SC_{ref}$ values from BE have a range centering at a slightly higher value (0.12–0.15 DU when selecting 10–1 percentile of the data distri-

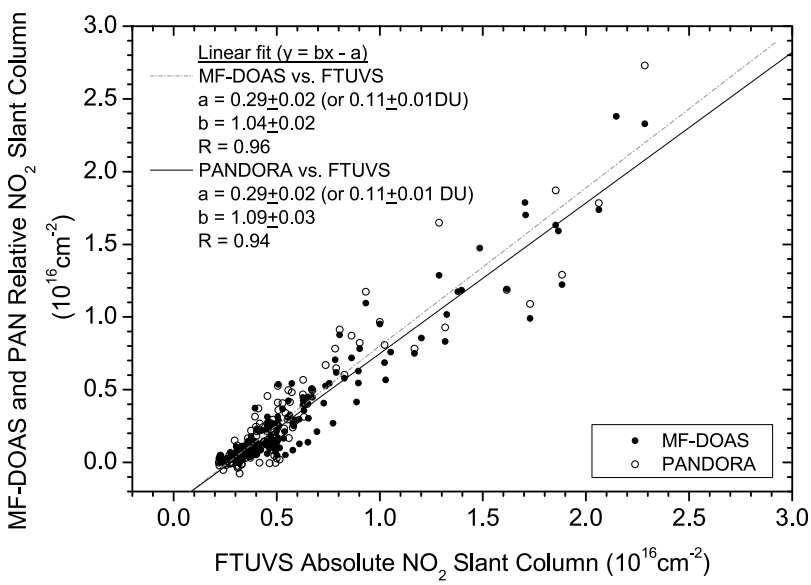


**Figure 7.** Linear correlation of the relative $NO_2$ slant columns from MF-DOAS and Pandora versus the absolute $NO_2$ slant columns from FTUVS. The slopes, $b$, are close to 1 for both cases. The negative intercepts of the linear fits, $a$, indicate the amounts of $NO_2$ in the high-Sun references used in MF-DOAS and Pandora retrieval.

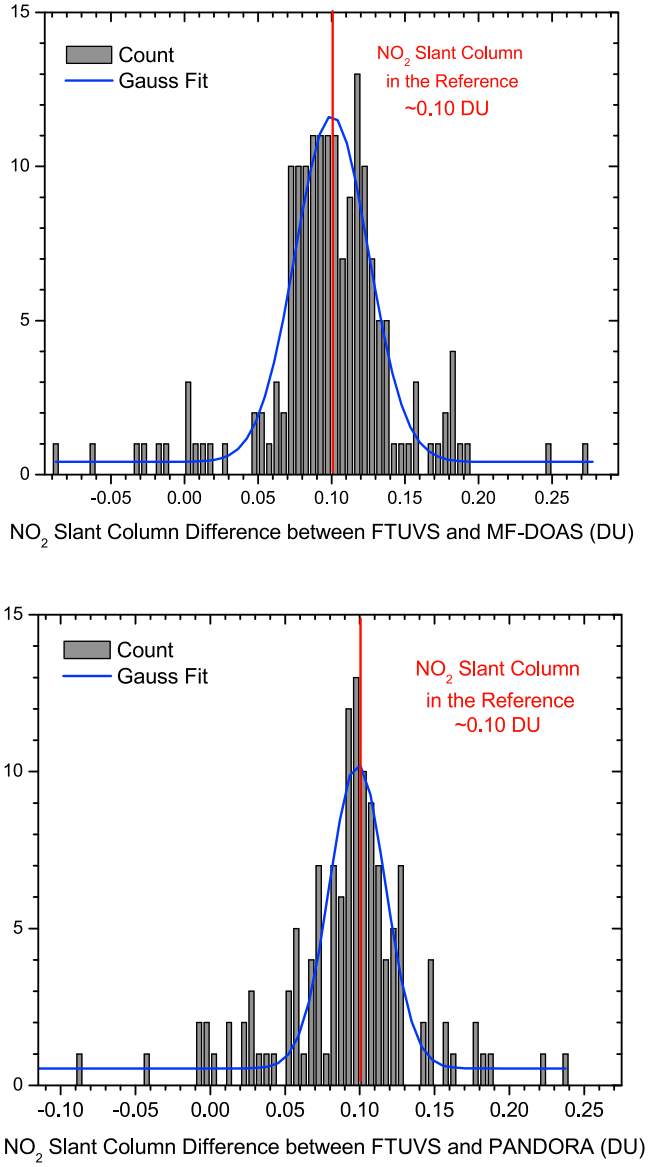


**Figure 8.** Histograms of the $NO_2$ slant columns in the high-Sun reference determined by the difference between the FTUVS absolute slant columns and the relative slant columns from MF-DOAS and Pandora. The peak center of the Gaussian fits implies the amount of $NO_2$ in the high-Sun reference.

bution given by *Herman et al.* [2009, Figure 10]). The MLE method requires that the minimum $C_{NO_2}$ is a constant during a portion of the measurement period. The BE method requires assumptions of the minimal $C_{NO_2}$, to be 0.1 DU in this case, during at least some part of the field campaign. Both methods work the best during extended campaigns with long data records (e.g., at GSFC as shown by *Herman et al.* [2009]) or at clean locations with very low tropospheric $NO_2$. The calibration through comparison with FTUVS measurements does not involve any of these assumptions (the assumption of the partition between stratospheric and tropospheric $NO_2$ is shown to have only a small impact of less than 0.01 DU on the calibration result as discussed in section 4.1) and works as a validation of the two calibration methods mentioned above. The agreement shown in Table 2 during TMF campaign with a period of only 11 days, therefore, confirms that TMF, though close to the Los Angeles basin, is a fairly clean observation site and can be free of pollution in the troposphere during some days. The calibration results are also very close to the nominal mid-latitude stratospheric $NO_2$ column of 0.1 DU. For the rest of this manuscript, the data from MF-DOAS and Pandora are calibrated with $SC_{ref}$ = 0.105 DU according to the FTUVS calibration method.

## 5. Vertical Column Results and Discussion

### 5.1. Diurnal Variation Comparison

[28] For direct Sun measurements, the slant column results can be easily converted into vertical column data through the geometrically determined AMF. All three data sets use the same method to calculate AMF [*Herman et al.*, 2009]. Any discrepancy originating from different AMF calculations at high SZAs is thus minimized. Since the FTUVS measurement cycle consists of two 17 min integration time periods for the opposite limbs, the average AMF during the short transition time between two limb measurements (at most a couple of minutes) was used for the corresponding $C_{NO_2}$ data. The resulting $C_{NO_2}$ data during this field campaign from all three instruments are plotted together in Figures 9 and 10.

[29] To facilitate the comparisons, the MF-DOAS (blue) and Pandora (red) data in Figure 9 were averaged during 17 min periods around each FTUVS data point (with an apparent time resolution of ~17 min). The error bars for FTUVS column data come from the spectral fit uncertainty. The error bars for MF-DOAS and Pandora data are the root-sum-square of two components, the standard deviation of the measured $NO_2$ vertical columns during the 17 min averaging period (up to 0.02 DU for MF-DOAS and up to 0.05 DU for Pandora) and the calibration uncertainty (0.01 DU divided by AMF). The measurement precision for each slant column data point (~0.01 DU) becomes very small after averaging in the vertical columns and is not shown here. For example, the averaging period typically covers a few hundred MF-DOAS data points (tens of data points for days when the instrument was operated alternately between the direct Sun mode and scattered-sky MAX-DOAS modes). The systematic errors are not shown in the plot. For FTUVS, the systematic errors are ~10%, corresponding to ~0.01–0.03 DU depending on the $NO_2$ column abundance. For MF-DOAS and Pandora data, the systematic error mostly comes from the calibration uncertainty, which is estimated to be within 0.1 DU when using the Langley or

**Table 2.** Comparison of the Instrument Calibration Results of $SC_{ref}$, $NO_2$ Slant Column in the High-Sun Reference, From Three Different Methods[a]

| Calibration methods | MF-DOAS (DU) | Pandora (DU) |
|---|---|---|
| FTUVS absolute method | 0.105 | 0.105 |
| Langley method | 0.12 | 0.12 |
| Bootstrap method | 0.12~0.15 | 0.12~0.15 |

[a]Values for Langley and bootstrap methods are taken from *Herman et al.* [2009].

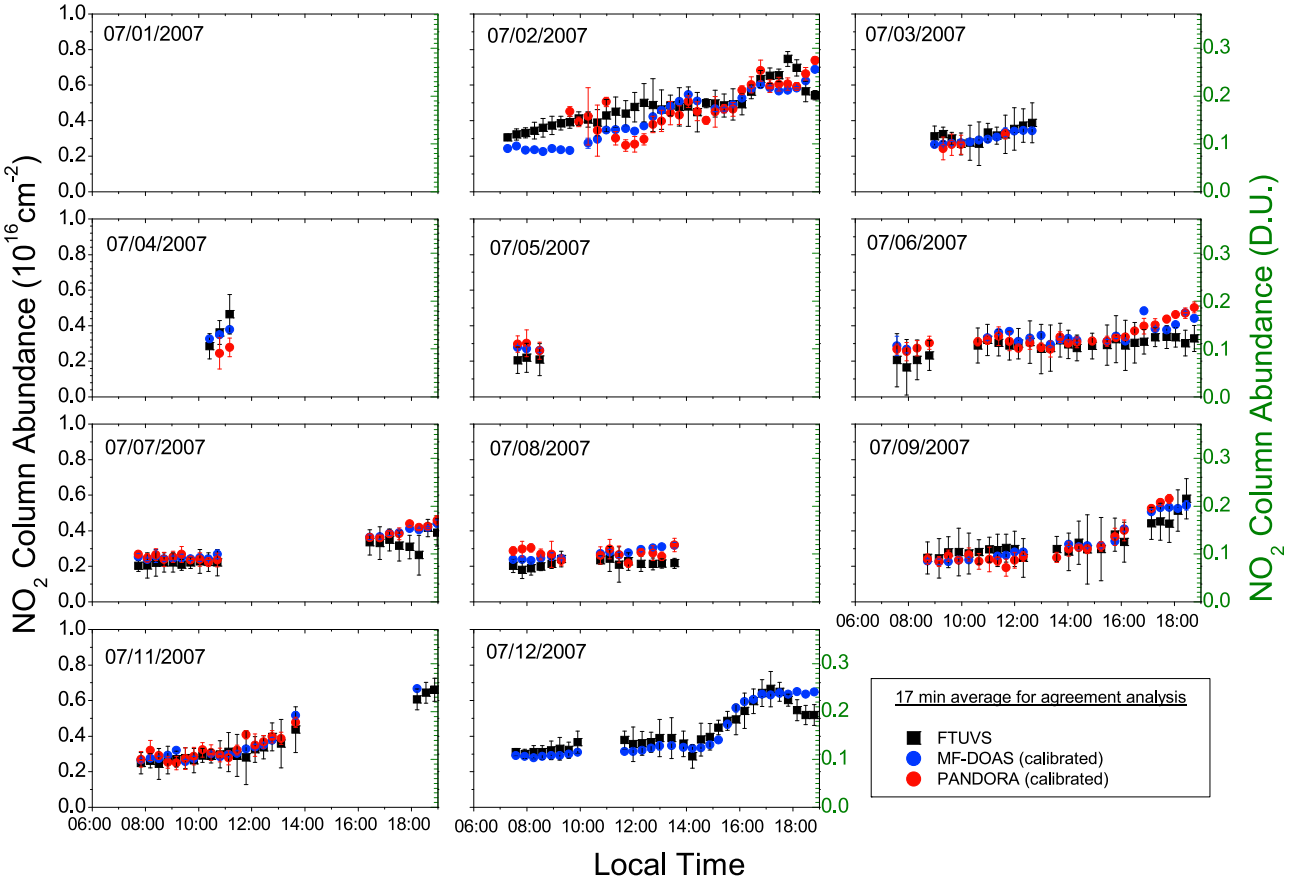


**Figure 9.** Comparison of $NO_2$ total vertical column abundances from three instruments. The data from MF-DOAS and Pandora are calibrated using the absolute measurement results from the high-resolution FTUVS. Only 17 min average data around each FTUVS measurement time are shown. For the complete data comparison, see Figure 10.

bootstrap method and leads to an uncertainty of (0.1/AMF) DU in the calibrated vertical column. To show the temporal behavior of $C_{NO_2}$, especially during periods when FTUVS data were not available, in Figure 10, the Pandora data (red) with an interval of a few minutes are used while the MF-DOAS data (blue) are 1 min averages (the original data have very fine time resolution and can dominate the plots). The error bars (except FTUVS data) are omitted in Figure 10 to avoid being overcrowded. Figure S2 included in the auxiliary material is equivalent to Figure 10 but with error bars for all data included.

[30] For reasons discussed above, there were several days during the campaign during which little or no data were available for one or more of the instruments. On 1 July, MF-DOAS was not fully configured and Pandora was undergoing initial alignment, which is reflected by the relatively large scatter in the Pandora data (Figure 10). The Pandora data during this day are not included in the calibration study discussed in section 4.1 or the overall comparison presented in sections 5.2 and 5.3. FTUVS data were unavailable during most of the day on 4 and 5 July because of heavy clouds. During the late afternoons of 3, 8, and 11 July and the midday of 7 July, multiple instrument alignments were required for FTUVS. The corresponding data were also excluded as mentioned in section 3.

[31] As shown in Figures 9 and 10, during most days, $C_{NO_2}$ from all instruments agree well. In particular, the diurnal variation patterns of the 17 min averaged data show excellent agreement. For most data points, the error bar ranges of all data sets overlap. In Figure 10 with higher time resolution, MF-DOAS data show somewhat less scatter than the Pandora data after 1 min averaging. Figure S2 in the auxiliary material shows that they correlate very well in most cases within the error ranges.

[32] Notable differences between data sets occur in two cases:

[33] 1. The end-of-day data of FTUVS, especially on days with high $NO_2$ levels, are often slightly lower than other data sets (e.g., the last one or two points on 2, 6, 11, and 12 July). As mentioned earlier in the experimental section, the total column retrieval algorithm of FTUVS uses an assumed partition of $NO_2$ between the troposphere and the stratosphere (tropospheric $NO_2$ contributes ~25% to the total column). The sensitivity of $C_{NO_2}$ retrieval results to this assumption is minimized after the high-pressure convolution. However, in cases with high tropospheric $NO_2$, the difference between the assumed and the true partition could introduce an underestimation of $C_{NO_2}$. In contrast, if the troposphere is even cleaner than our assumption, a small overestimation could occur. This effect should be, however, very small (generally within a

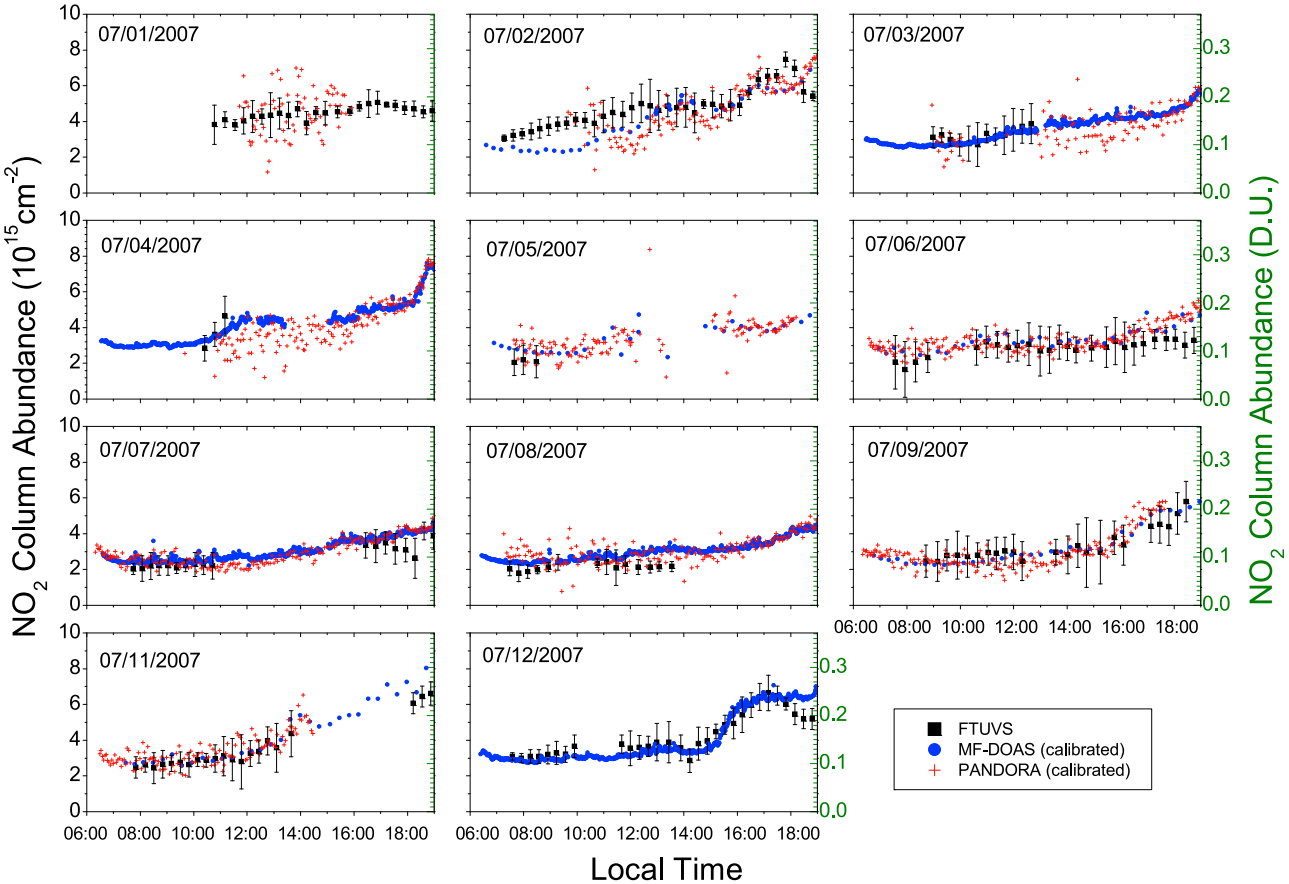


**Figure 10.** Comparison of $NO_2$ total vertical column abundances from three instruments during the 11 day field campaign. The data from MF-DOAS (1 min average) and Pandora are calibrated using the absolute measurement results from the high-resolution FTUVS. Days with fewer MF-DOAS data points were days when the instrument was taking direct Sun and scattered-sky measurements alternately.

couple percent). While TMF is relatively clean, in some late afternoons, polluted air masses can be transported to the site leading to higher tropospheric $NO_2$. The resulting underestimation of FTUVS $C_{NO_2}$ could reach up to ~10% for polluted cases. Since this small discrepancy occurs at the end of the day when $NO_2$ levels are high, this source of systematic error may be responsible.

[34] 2. Several FTUVS data points on the morning of 2 July (0800–1000 LT) are higher than the MF-DOAS data (with a difference of 0.5–1.5 × $10^{15}$ $cm^{-2}$). Unfortunately, there are no Pandora data available during this period for comparison. Since the Pandora data typically has a combined error bar on the order of ±1 × $10^{15}$ $cm^{-2}$, it is likely that both FTUVS and MF-DOAS data would fall in the Pandora data range if Pandora data were available. The Pandora data also show multiple peaks of $C_{NO_2}$ in the diurnal variation on 2 July, most of which are also reflected in the time series of MF-DOAS and FTUVS data with relatively weaker variations.

### 5.2. Linear Correlation of the Vertical Columns

[35] In order to assess the overall agreement among these measurements, an orthogonal least square linear correlation (also known as the "total" least squares regression) as well as the standard linear fit are applied. In Figure 11, the FTUVS absolute measurement results are plotted on the horizontal axis, and the calibrated vertical columns from MF-DOAS and Pandora (17 min averaged data as shown in Figure 9) are plotted on the vertical axis. As mentioned earlier, the horizontal error bars are the 1 $\sigma$ precision from the FTUVS spectral retrieval. The vertical error bars for MF-DOAS and Pandora data are combinations of standard deviation of the data during the 17 min averaging period and the calibration uncertainty (the measurement precision becomes very good after averaging).

[36] The advantage of the orthogonal linear fit over the standard linear fit is that it takes into account the deviation of the data points in both $x$ and $y$ directions from the fitted line and the error bars in both directions ($\sigma_x$ and $\sigma_y$) are weighted. Instead of minimizing the sum of the squared vertical distance from the data points to the fitted line, the orthogonal linear fit minimizes the sum of the squared orthogonal distance between the data points ($x_i$, $y_i$) and the prediction ($X_i$, $Y_i$). The intercept $a$ and slope $b$ are obtained by minimizing $\chi^2 = \sum_i [(X_i - x_i)^2/\sigma_{xi}^2 + (Y_i - y_i)^2/\sigma_{yi}^2]$ [*Press et al.*, 1992; *Reed*, 1989; 1992; *York*, 1966].

[37] The linear correlation coefficients in Figure 11 are good for both data sets ($R$ = 0.86 and 0.80). For MF-DOAS versus FTUVS, both orthogonal and standard fits are very

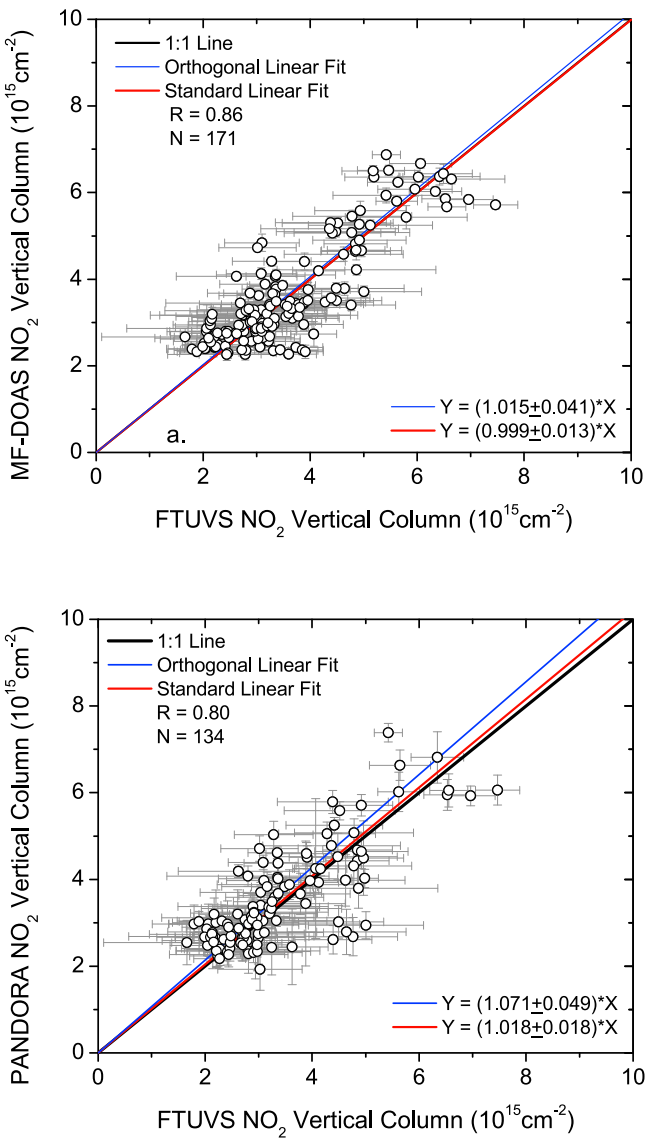


**Figure 11.** Linear correlation of the $NO_2$ vertical columns: (top) MF-DOAS versus FTUVS and (bottom) Pandora versus FTUVS. The error bars of MF-DOAS and Pandora data include the precision after averaging and the standard deviation of the data during the 17 min average. Both error bars in $x$ and $y$ directions are weighted in the orthogonal fit.

close to the one-to-one line. The orthogonal fit gives a slope of (1.5 ± 4.1)% and the slope from the standard fit is within this range. It is thus suggested that MF-DOAS data are about (1.5 ± 4.1)% larger than FTUVS measurements. The fits for Pandora versus FTUVS give two slope ranges slightly wider with partial overlapping. By combining the two slope ranges, Pandora data are shown to be about (6.0 ± 6.0)% larger than FTUVS data.

### 5.3. Histograms of Measurement Differences

[38] Histograms of the differences between various measurements are useful in assessing the statistical distributions of the ensemble. For the data sets in Figure 11, the horizontal error bar is on the order of $\pm 1 \times 10^{15}$ cm$^{-2}$ and the range of the scatter is large (the typical $y$ range at a given $x$ value is as large as $3 \times 10^{15}$ cm$^{-2}$). The range of $C_{NO_2}$ (5~6 × $10^{15}$ cm$^{-2}$ from minimum to maximum) is not much larger than the data scatter range, which leads to the relatively large uncertainty range of the linear fit slopes in Figure 11. In such a case, histograms can be used to confirm linear correlation results. Unlike the orthogonal linear fit for which the data are weighted by the uncertainties, the error bars are not considered in the histograms.

[39] Figure 12 shows the histograms of the $C_{NO_2}$ difference between measurements from different instruments. Figures 12a and 12b show the percentage difference, which is equivalent to a standard linear fit (no error bars weighted) through zero. Figures 12c and 12d show the absolute difference, equivalent to a standard fit with a slope of unity. The Gaussian fits of the histograms are also plotted to show the center and the sigma range. The differences among these measurements are shown to have near-Gaussian distributions and are random in nature. The centers of the Gaussian fits (Figures 12a and 12b) to these histograms suggest that MF-DOAS and Pandora data are ~3% and ~5% larger than FTUVS. These values are both well within the value ranges suggested by the linear correlation studies ((1.5 ± 4.1)% and (6.0 ± 6.0)%).

[40] In terms of the absolute difference in $C_{NO_2}$, MF-DOAS and Pandora data are (0.13 ± 0.45) × $10^{15}$ and (0.23 ± 0.43) × $10^{15}$ cm$^{-2}$ larger than FTUVS data (suggested by the centers of the Gaussian fits in Figures 12c and 12d). Changing the size of the bins in the histograms leads to negligible changes in these values. Assuming the absolute measurements derived from the FTUVS to be the true $NO_2$ column abundances, the standard deviations of the MF-DOAS and Pandora data sets from the FTUVS data during the entire campaign are found to be small, 6.36 × $10^{14}$ cm$^{-2}$ and 7.36 × $10^{14}$ cm$^{-2}$, respectively.

### 5.4. Comparison Between MF-DOAS and Pandora Measurements

[41] Although the two data sets generally agree very well in Figure 10, the midday Pandora data appear to be slightly smaller on some days (e.g., 4 and 7 July). Figure 6 shows that Pandora slant columns are about 5% larger than MF-DOAS data with a small negative intercept of 2.65 × $10^{14}$ cm$^{-2}$. Therefore, the correlation between the calibrated $C_{NO_2}$ from these two instruments is expected to be

$$[NO_2]_{Pandora} = 1.05\left([NO_2]_{MF\text{-}DOAS}\right) - \frac{2.65 \times 10^{14} + 0.05(SC_0)}{AMF}, \quad (5)$$

where $SC_0$ is the $NO_2$ slant column in the high-Sun reference (0.105 DU) and $[NO_2]$ is the $NO_2$ vertical column abundance. Depending on the magnitudes of $[NO_2]$ and the AMF, the Pandora $NO_2$ columns could be larger or smaller than the MF-DOAS data. When the value of the negative term on the right side of (5) is 5% of $[NO_2]$, the two measurements are the same. At the end of the day with high $[NO_2]$ and large AMFs, the Pandora data could be slightly larger (less than 5%) than the MF-DOAS data. Near noontime when the AMF is about 1, the effect of the negative term in (5) is maximized. The Pandora data could be slightly smaller than MF-DOAS data. In the scatterplot of Pandora data versus MF-DOAS data

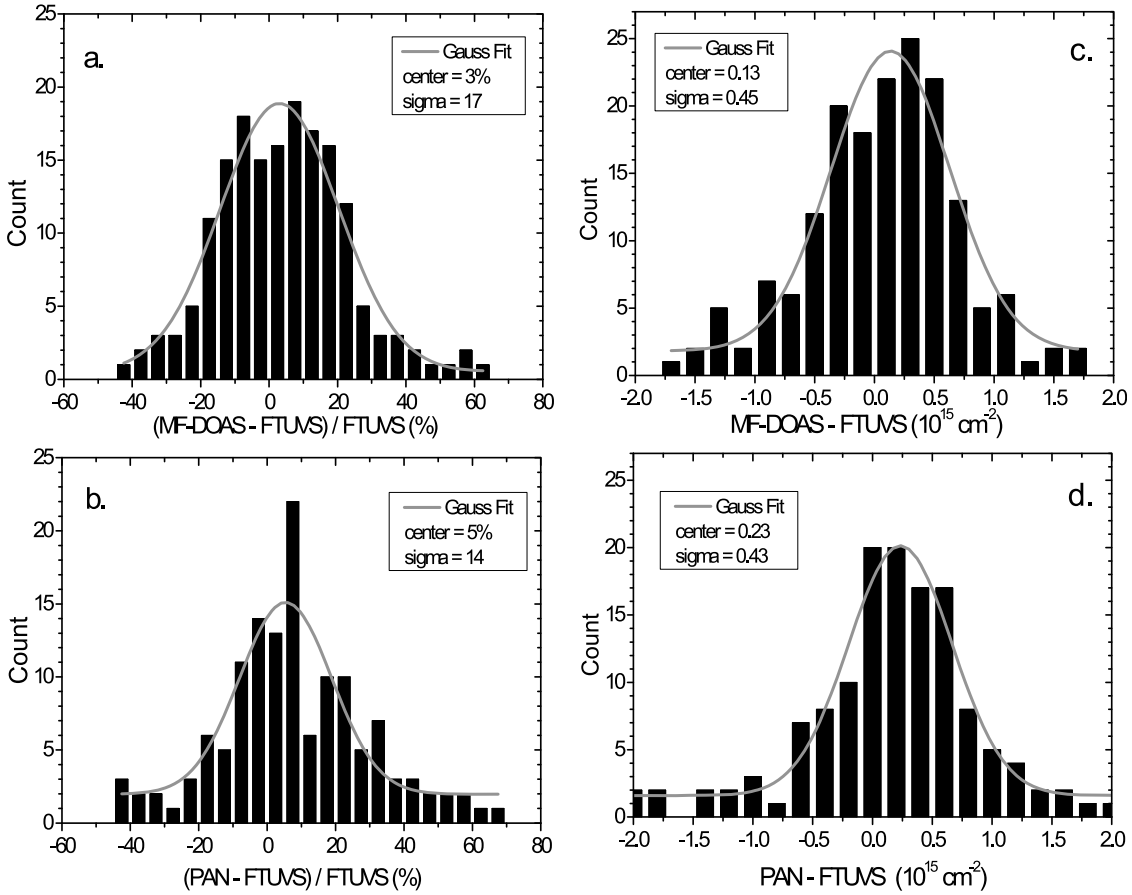


**Figure 12.** Histograms of differences of $NO_2$ vertical columns: (a and c) MF-DOAS versus FTUVS and (b and d) Pandora versus FTUVS. Figures 12a and 12b show the percentage differences between vertical columns from different instruments. Figures 12c and 12d show the absolute differences.

(Figure 13a), two straight lines are calculated on the basis of (5), with AMFs of 5 (during the last hour of the day) and 1.01 (noon). The scatters are color coded according to AMFs. The straight line with end-of-day AMF (blue) fits the colored data at relatively large AMFs, while the other line with noontime AMF (red) fits very well the data at low AMFs (in black). The AMF variation of the difference between these two measurements, (Pandora minus MF-DOAS), is also seen in Figure 13b. The value of (Pandora minus MF-DOAS) tends to be positive at high AMFs. At low AMFs, it has much larger variability and tends to be more negative. Since the systematic error for both instruments is about 0.1 DU, $2.69 \times 10^{15}$ cm$^{-2}$ at low AMFs, the $NO_2$ vertical column difference between these measurements is within the systematic error for 99.9% of the data.

### 5.5. Possible Sources of Differences

[42] While the diurnal variations of $C_{NO_2}$ from all three instruments generally agree well (Figure 9), the measurements from MF-DOAS and Pandora appear to be statistically slightly higher than the FTUVS measurements (Figures 11–13) after correction for the $NO_2$ column in the reference spectra. A few possible reasons for these differences are discussed below.

[43] The first possible cause of differences is the usage of different $NO_2$ cross sections. As shown in sections 2.1 and 2.2, both MF-DOAS and Pandora used $NO_2$ cross sections from *Harder et al.* [1997], which covers a wider spectral region that is required for the grating spectrometers. These cross sections cannot be used for FTUVS since the moderate spectral resolution (0.15 cm$^{-1}$) is not high enough to accurately match the Doppler shifted (~0.28 cm$^{-1}$) spectra from the east and west limbs of the Sun. The FTUVS $NO_2$ reference was derived from high-resolution (0.06 cm$^{-1}$) cross section measurements by *Nizkorodov et al.* [2004]. To compare the two sets of cross sections, the high-resolution data from *Nizkorodov et al.* [2004] that were measured at low pressure and various temperatures were interpolated to 1 atmosphere pressure and 238 K (similar conditions of the measurements by *Harder et al.* [1997]). The comparison between these cross section data show very small differences, mostly within 2%, with a maximum of 4% (see Figure S3 in the auxiliary material). The differences between $NO_2$ columns from FTUVS and the grating spectrometers that are caused by differences in cross sections are thus expected to be within a few percent.

[44] Second, as described in section 2.2, an average temperature of 238 K is assumed for the $NO_2$ absorption cross sections used in the MF-DOAS and Pandora retrievals, while FTUVS uses a temperature profile based on the standard atmosphere. The FTUVS $NO_2$ cross sections are calculated on the basis of the $NO_2$ density-weighted average temper-

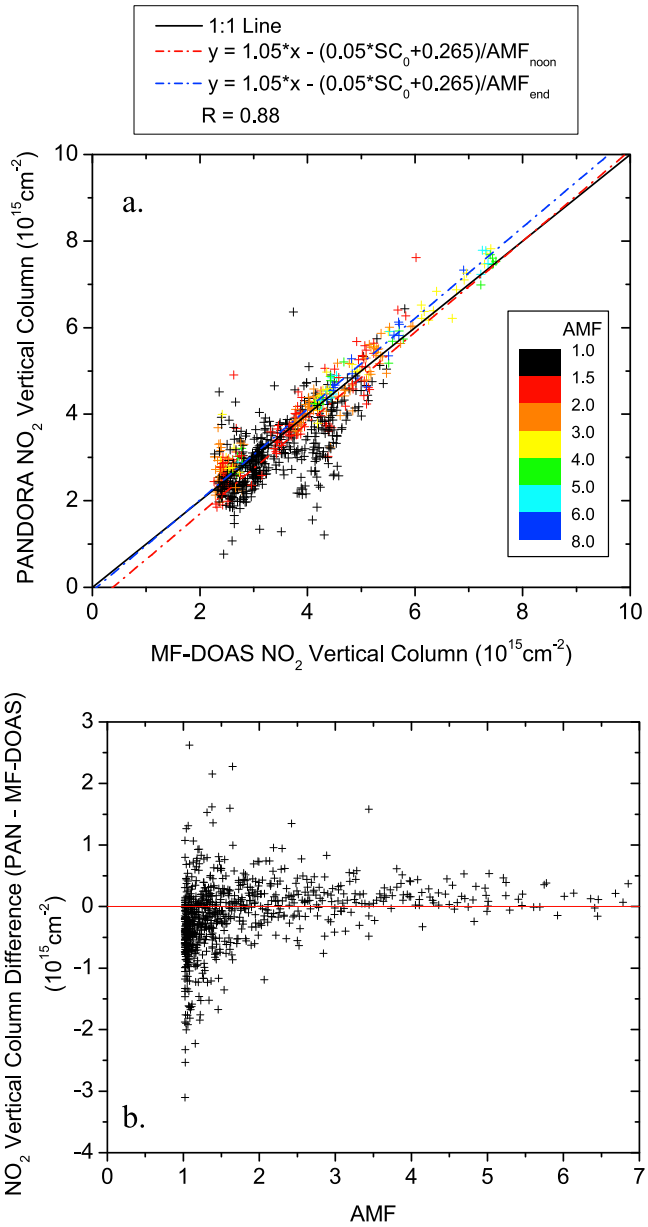


**Figure 13.** Comparison of $NO_2$ vertical columns measured with Pandora and MF-DOAS. (a) Pandora data versus MF-DOAS data. (b) The AMF variation of the difference between these two measurements (Pandora minus MF-DOAS). The MF-DOAS 1 min average data were interpolated to the nearest Pandora measurement time.

ature in the atmosphere. The sensitivity studies suggest that retrieved FTUVS $NO_2$ columns would increase by about 1% if the weighted average temperature was replaced with a constant temperature of 238 K.

[45] The third possible source of discrepancy arises from a systematic error in the FTUVS total column retrieval algorithm, when the troposphere is significantly more polluted than our a priori assumption. As discussed in section 5.1, when the tropospheric contribution to the total column is significantly larger than the assumed stratospheric/tropospheric partition (the ratio of the stratospheric partial column to the tropospheric partial column) in building the total atmospheric $NO_2$ absorption cross sections, the $NO_2$ column could be slightly underestimated. While this underestimation is small, in cases when polluted air mass is transported to TMF so that the tropospheric $NO_2$ contribute to at least half to the total column, this underestimation could reach 10%. Table Mountain generally has low tropospheric $NO_2$. However, when the wind favors transport of air with high $NO_2$ from Los Angeles urban pollution to the mountains in the late afternoon, a significant underestimation cannot be ruled out. In Figure 9, the late afternoon $NO_2$ abundance on 2 July and 9–12 July, for example, appears to be higher than on other days, implying that the tropospheric $NO_2$ is higher than usual cases. The FTUVS data during the last hour of these days is also shown to be lower than the other measurements. We calculated back trajectories with the NOAA Hybrid Single-Particle Lagrangian Integrated Trajectory (HYSPLIT) model, but it was not able to describe a reasonable air mass transport route because of the complex nature of the topography in the TMF area. Thus, the exact effect of transport is not known.

[46] The fourth cause of the measurement difference could be the AMF used by different groups. The three involved instruments have significantly different time resolutions. A typical measurement cycle for FTUVS takes about 17 min for each limb. The AMF is calculated at the beginning and the end of the measurement of each limb. The AMF used for each data point is calculated on the basis of the linear mean of the AMFs at the end of the first limb and the beginning of the second limb that are often a few minutes apart. This approximation of using linear mean instead of exponential interpolation could, in principle, introduce a small error (leading to smaller $C_{NO_2}$) when the AMF is changing rapidly at the very end of the day. During this field campaign, the largest AMF for FTUVS data is about 5. The possible error due to this approximation in FTUVS AMF averaging is believed to be very small, less than 1%.

## 6. Conclusions

[47] During an intercomparison campaign at JPL's Table Mountain Facility in July 2007, $NO_2$ total columns, $C_{NO_2}$, were measured using three independent direct Sun viewing instruments. The JPL FTUVS, a high-resolution Fourier transform spectrometer, measured absolute $I_0$-independent slant columns while the lower-resolution grating spectrometers, Pandora and MF-DOAS, measured differential $NO_2$ slant columns and then used field calibrations to produce absolute slant columns. The cross correlation of absolute slant columns from the FTUVS and differential slant columns from colocated MF-DOAS and Pandora provides an accurate and precise calibration validation for the latter two instruments. The statistic studies show a calibration uncertainty of 0.01 DU, which is much smaller than the calibration uncertainty of MLS or BE method (~0.1 DU). The calibrations using the modified Langley and bootstrap methods (MLE and BE) are shown to be consistent with the calibrations derived from comparison with FTUVS within experimental errors. While the accuracy of BE method requires short periods of extremely low levels of tropospheric $NO_2$, the MLE method requires portions of the data to have a nearly

constant $C_{NO_2}$. Since TMF usually has very low tropospheric $NO_2$, the two methods have comparable accuracy and are shown to be both valid during this TMF campaign.

[48] The calibrated slant columns are converted into vertical columns via geometrical AMFs. The vertical column data from all three instruments agree very well. Detailed statistical studies suggest that both MF-DOAS and Pandora data sets agree with FTUVS data to within a few percent. They are found to be (1.5 ± 4.1)% and (6.0 ± 6.0)% larger than FTUVS measurements. The absolute $C_{NO_2}$ differences of (MF-DOAS minus FTUVS) and (Pandora minus FTUVS) are found to be $(0.13 \pm 0.45) \times 10^{15}$ and $(0.23 \pm 0.43) \times 10^{15}$ $cm^{-2}$, respectively. All these differences are well within the systematic uncertainty ranges. Possible sources of differences include the temperature profiles used in calculating the $NO_2$ absorption cross sections, the assumed stratospheric/tropospheric $NO_2$ partitioning in the FTUVS retrieval algorithm, and errors associated with the rapidly changing AMFs at sunset.

[49] **Acknowledgments.** We acknowledge the support of the NASA Upper Atmosphere Research and Aura Validation programs to each of these groups: JPL, WSU, and GSFC. We also wish to thank the staff at JPL's Table Mountain Facility, especially Pam Glatfelter and Bruce Williamson, for their exceptional support during the intercomparison campaign. The WSU group thanks Robert Gibson for help in the field. This research was carried out at the Jet Propulsion Laboratory, California Institute of Technology; Washington State University; and the Goddard Space Flight Center under contract to the National Aeronautics and Space Administration.

## References

Boersma, K. F., et al. (2007), Near-real time retrieval of tropospheric $NO_2$ from OMI, *Atmos. Chem. Phys.*, *5*, 2311–2331.

Brasseur, G. P., D. A. Hauglustaine, S. Walters, P. J. Rasch, J. F. Muller, C. Granier, and X. X. Tie (1998), MOZART, a global chemical transport model for ozone and related chemical tracers: 1. Model description, *J. Geophys. Res.*, *103*, 28,265–28,289, doi:10.1029/98JD02397.

Brewer, A. W., C. T. McElroy, and J. B. Kerr (1973), Nitrogen dioxide concentrations in the atmosphere, *Nature*, *246*(5429), 129–133, doi:10.1038/246129a0.

Bucsela, E. J., E. A. Celarier, M. O. Wenig, J. F. Gleason, J. P. Veefkind, K. F. Boersma, and E. J. Brinksma (2006), Algorithm for $NO_2$ vertical column retrieval from the ozone monitoring instrument, *IEEE Trans. Geosci. Remote Sens.*, *44*(5), 1245–1258, doi:10.1109/TGRS.2005.863715.

Cageao, R. P., J. Blavier, J. P. McGuire, Y. Jiang, V. Nemtchinov, F. P. Mills, and S. P. Sander (2001), High-resolution Fourier-transform ultraviolet-visible spectrometer for the measurement of atmospheric trace species: Application to OH, *Appl. Opt.*, *40*(12), 2024–2030, doi:10.1364/AO.40.002024.

Cede, A., J. Herman, A. Richter, N. Krotkov, and J. Burrows (2006), Measurements of nitrogen dioxide total column amounts at Goddard Space Flight Center using a Brewer spectrometer in direct Sun mode, *J. Geophys. Res.*, *111*, D05304, doi:10.1029/2005JD006585.

Celarier, E. A., et al. (2008), Validation of Ozone Monitoring Instrument nitrogen dioxide columns, *J. Geophys. Res.*, *113*, D15S15, doi:10.1029/2007JD008908.

Cheung, R., K. F. Li, S. Wang, T. J. Pongetti, R. P. Cageao, S. P. Sander, and Y. L. Yung (2008), Atmospheric hydroxyl radical (OH) abundances from ground-based ultraviolet solar spectra: An improved retrieval method, *Appl. Opt.*, *47*, 6277–6284, doi:10.1364/AO.47.006277.

Crutzen, P. J. (1970), The influence of nitrogen oxides on the atmospheric ozone content, *Q. J. R. Meteorol. Soc.*, *96*, 320–325, doi:10.1002/qj.49709640815.

Harder, J. W., J. W. Brault, P. V. Johnson, and G. H. Mount (1997), Temperature dependent $NO_2$ cross sections at high spectral resolution, *J. Geophys. Res.*, *102*, 3861–3879, doi:10.1029/96JD03086.

Herman, J., A. Cede, E. Spinei, G. Mount, M. Tzortziou, and N. Abuhassan (2009), $NO_2$ column amounts from ground-based Pandora and MFDOAS spectrometers using the direct-Sun DOAS technique: Intercomparisons and application to OMI validation, *J. Geophys. Res.*, *114*, D13307, doi:10.1029/2009JD011848.

Hönninger, G., H. Leser, O. Sebastian, and U. Platt (2004), Ground-based measurements of halogen oxides at the Hudson Bay by active longpath DOAS and passive MAX-DOAS, *Geophys. Res. Lett.*, *31*, L04111, doi:10.1029/2003GL018982.

Ionov, D. V., Y. M. Timofeyev, P. Sinyakov, V. K. Semenov, F. Goutail, J.-P. Pommereau, E. J. Bucsela, E. A. Celarier, and M. Kroon (2008), Ground-based validation of EOS-Aura OMI $NO_2$ vertical column data in the midlatitude mountain ranges of Tien Shan (Kyrgyzstan) and Alps (France), *J. Geophys. Res.*, *113*, D15S08, doi:10.1029/2007JD008659.

Iwagami, N., S. Inomata, I. Murata, and T. Ogawa (1995), Doppler detection of hydroxyl column abundance in the middle atmosphere, *J. Atmos. Chem.*, *20*(1), 1–15, doi:10.1007/BF01099915.

Kramer, L. J., R. J. Leigh, J. J. Remedios, and P. S. Monks (2008), Comparison of OMI and ground-based in situ and MAX-DOAS measurements of tropospheric nitrogen dioxide in an urban area, *J. Geophys. Res.*, *113*, D16S39, doi:10.1029/2007JD009168.

Li, K.-F., R. P. Cageao, E. M. Karpilovsky, F. P. Mills, Y. L. Yung, J. S. Margolis, and S. P. Sander (2005), OH column abundance over Table Mountain Facility, California: AM-PM diurnal asymmetry, *Geophys. Res. Lett.*, *32*, L13813, doi:10.1029/2005GL022521.

Logan, J. A., M. J. Prather, S. C. Wofsy, and M. B. McElroy (1981), Tropospheric chemistry: A global perspective, *J. Geophys. Res.*, *86*, 7210–7254, doi:10.1029/JC086iC08p07210.

McPeters, R., M. Kroon, G. Labow, E. Brinksma, D. Balis, I. Petropavlovskikh, J. P. Veefkind, P. K. Bhartia, and P. F. Levelt (2008), Validation of the Aura Ozone Monitoring Instrument total column ozone product, *J. Geophys. Res.*, *113*, D15S14, doi:10.1029/2007JD008802.

Mills, F. P., R. P. Cageao, V. Nemtchinov, Y. Jiang, and S. P. Sander (2002), OH column abundance over Table Mountain Facility, California: Annual average 1997–2000, *Geophys. Res. Lett.*, *29*(15), 1742, doi:10.1029/2001GL014151.

Murphy, D., D. Fahey, M. Proffitt, S. Liu, C. Eubank, S. Kawa, and K. Kelly (1993), Reactive odd nitrogen and its correlation with ozone in the lower stratosphere and upper troposphere, *J. Geophys. Res.*, *98*, 8751–8773, doi:10.1029/92JD00681.

Nizkorodov, S. A., S. P. Sander, and L. R. Brown (2004), Temperature and pressure dependence of high-resolution air-broadened absorption cross sections of $NO_2$ (415–525 nm), *J. Phys. Chem. A*, *108*, 4864–4872, doi:10.1021/jp049461n.

Platt, U., and J. Stutz (2008), *Differential Optical Absorption Spectroscopy: Principles and Applications*, 597 pp., Springer, Heidelberg, Germany.

Press, W. H., et al. (1992), *Numerical Recipes in C: The Art of Scientific Computing*, 2nd ed., Cambridge Univ. Press, Cambridge, U. K.

Reed, B. C. (1989), Linear least-squares fits with errors in both coordinates, *Am. J. Phys.*, *57*(7), 642–646, doi:10.1119/1.15963.

Reed, B. C. (1992), Linear least-squares fits with errors in both coordinates. II: Comments on parameter variances, *Am. J. Phys.*, *60*(1), 59–62, doi:10.1119/1.17044.

Roscoe, H. K., et al. (1999), Slant column measurements of $O_3$ and $NO_2$ during the NDSC intercomparison of zenith-sky UV-visible spectrometers in June 1996, *J. Atmos. Chem.*, *32*, 281–314, doi:10.1023/A:1006111216966.

Seinfeld, J. H., and S. N. Pandis (1998), *Atmospheric Chemistry and Physics—From Air Pollution to Climate Change*, John Wiley, New York.

van der A, R. J., H. J. Eskes, K. F. Boersma, T. P. C. van Noije, M. van Roozendael, I. De Smedt, D. H. M. U. Peters, and E. W. Meijer, (2008), Trends, seasonal variability and dominant $NO_x$ source derived from a ten year record of $NO_2$ measured from space, *J. Geophys. Res.*, *113*, D04302, doi:10.1029/2007JD009021.

Wang, S., et al. (2008), Validation of Aura Microwave Limb Sounder OH measurements with Fourier Transform Ultra-Violet Spectrometer total OH column measurements at Table Mountain, California, *J. Geophys. Res.*, *113*, D22301, doi:10.1029/2008JD009883.

Wenig, M., S. Kuhl, S. Beirle, E. Bucsela, B. Jahne, U. Platt, J. Gleason, and T. Wagner (2004), Retrieval and analysis of stratospheric $NO_2$ from the Global Ozone Monitoring Experiment, *J. Geophys. Res.*, *109*, D04315, doi:10.1029/2003JD003652.

Wenig, M. O., A. M. Cede, E. J. Bucsela, E. A. Celarier, K. F. Boersma, J. P. Veefkind, E. J. Brinksma, J. F. Gleason, and J. R. Herman (2008), Validation of OMI tropospheric $NO_2$ column densities using direct-Sun mode Brewer measurements at NASA Goddard Space Flight Center, *J. Geophys. Res.*, *113*, D16S45, doi:10.1029/2007JD008988.

Wittrock, F., H. Oetjen, A. Richter, S. Fietkau, T. Medeke, A. Rozanov, and J. P. Burrows (2004), MAX-DOAS measurements of atmospheric trace gases in Ny-Ålesund–Radiative transfer studies and their application, *Atmos. Chem. Phys.*, *4*, 955–966, doi:10.5194/acp-4-955-2004.

York, D. (1966), Least-squares fitting of a straight line, *Can. J. Phys.*, *44*, 1079–1086.

A. Cede, Earth System Science Interdisciplinary Center, University of Maryland, 5825 University Research Ct., College Park, MD 20740, USA.

J. Herman, NASA Goddard Space Flight Center, Bldg. 33, Code 916, Rm. E416, Greenbelt, MD 20771, USA.

G. H. Mount and E. Spinei, Laboratory for Atmospheric Research, Department of Civil and Environmental Engineering, Washington State University, Pullman, WA 99164, USA.

T. J. Pongetti, S. P. Sander, and S. Wang, Jet Propulsion Laboratory, California Institute of Technology, Mail Stop 183-901, 4800 Oak Grove Dr., Pasadena, CA 91109, USA. (shuhui.wang@jpl.nasa.gov)